Inorganic Chemistry Communications 140 (2022) 109407

Contents lists available at ScienceDirect

Inorganic Chemistry Communications

journal homepage: www.elsevier.com/locate/inoche

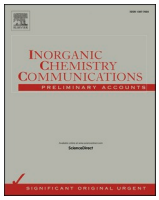

Short communication

Influence of the methods of synthesis and grain size distribution on XEOL spectra of $CaWO_4$:xTb^{3+}

E.A Mukhanova *, I.A. Pankin, O.E. Polozhentsev, P.D. Kuznetsova, V.A. Polyakov, A.V. Soldatov

Smart Materials Research Institute, Southern Federal University, Sladkova 178/24, 344090 Rostov-on-Don, Russia

ARTICLE INFO

Keywords:
XEOL
Scheelite
Tungstates
Size distribution

ABSTRACT

X-ray photodynamic therapy (XPDT) is one of the growing methods for the treatment of deep tumors. Substituted calcium tungstate $CaWO_4$ is one of the potential phosphors for a wide range of photosensitizers. In our work, we studied the possibility of replacing Ca^{2+} with Tb^{3+} in the scheelite structure and also the effect of the synthesis method on the particle size distribution. It was found that the synthesis and subsequent morphological differences between the samples lead to different intensities of luminescence. This can be used to improve the characteristics of composites for XPDT.

1. Introduction

Photodynamic therapy (PDT) is one of the promising methods for the treatment of tumors [1-4]. The advantages of this therapy are high selectivity for cancer cells and relatively safety without long-term side effects for the organism. But its implementation requires some special conditions, taking into account the tumor environment - a type of photosensitizer, radiation with a suitable wavelength for it, and the efficient production of reactive oxygen species (ROS) [4-7]. The advantage of X-ray PDT compared to the conventional method is its ability to affect deep tumors due to the significantly higher penetration capability of X-rays compared even with red lasers, which are known to have a greater penetration into tissue among all visible light [8,9]. In XPDT, it is also important to select a luminophore with a suitable wavelength of luminescence to activate a photosensitizer. The well-known pairs of luminophore photosensitizers are discussed in detail in reviews [10,11]. It can be noted that among inorganic phosphors there are not many compounds known in which optical luminescence can be excited by irradiation with X-ray or gamma radiation. Among the described in the literature, not all of them are used in the treatment of tumors because of the complexity of synthesis, including in the nano-scale state.

Calcium tungstate is well known as a scintillator, but it has a very broad peak with a low intensity [12-15]. For doped calcium tungstates with a scheelite structure, X-ray excited optical luminescence (XEOL) spectra with europium and terbium are described [16]. These phosphors have two emission regions corresponding to the WO_4^{2-} anion and lanthanide cation. The wider radiation area makes it easier to find a suitable photosensitizer. Doped samples have the following advantages: 1) Eu^{3+} and Tb^{3+} ions show intense red and green radiation, respectively, 2) their luminescence spectra consist of narrow bands [16].

The toxicity of complex compounds of terbium (III) and europium (III) is low [17]. They have been reported to have antibacterial properties [18]. The low cytotoxicity of Eu(III) is also confirmed in studies [19,20] using a suspension of Brassica napus plant cells. Cells were exposed to a solution of Eu (III) with a molar concentration of 0 to 200 μM, - about 75% of europium was immobilized by plant cells with the preservation of their vital functions. Europium hydroxide nanorods, which exhibit proangiogenic properties (promoting the growth of new blood vessels) properties, have shown a nontoxic nature in laboratory mice [21]. However, lanthanides, especially terbium (III) and europium (III), can replace calcium in their body structures and also react with calcium-binding proteins instead of calcium, [22] which can have negative consequences.

The synthesis of these materials can be carried out by the following methods: solid-state, sol–gel, coprecipitation, microwave-assisted, etc. [13,14,23-25]. The method of synthesis can significantly affect the size of particles, their morphology, and surface properties. All of these aspects are crucial for scintillating nanoparticles. For example, it is known that the luminescence intensity is significantly dependent on particle size [26]. These parameters can change the processes of charge transfer and lead to the appearance of quantum effects on the nanoscale state.

* Corresponding author.
E-mail address: kand@sfedu.ru (E.A Mukhanova).

https://doi.org/10.1016/j.inoche.2022.109407
Received 26 November 2021; Received in revised form 5 March 2022; Accepted 17 March 2022
Available online 1 April 2022
1387-7003/© 2022 Elsevier B.V. All rights reserved.

This relationship is usually not linear. Therefore, the purpose of this work was to study the influence of the different synthesis routes on the grain size distribution and the XEOL spectra of Tb^{3+}-doped tungstates.

2. Experimental

2.1. Methods of synthesis

2.1.1. Microwave-assisted synthesis

As starting materials, we used $CaCl_2$, $Na_2WO_4{\cdot}2H_2O$, $TbCl_3{\cdot}6H_2O$, and PEG-1000, and all were of analytical grade. $CaWO_4$:10 %Tb^{3+} nanocrystals were prepared by the microwave-assisted method as described in [27]. All reagents were placed in a quartz tube and dissolved in 10 ml of distilled water. The mixture was then vigorously stirred for 10 min to ensure that all reagents were evenly dispersed. Then the sealed quartz tube was put into the CEM Discover microwave reactor. The reaction was held for 30 min at 110° C and the microwave power output was 100 W. The maximum pressure was 274 kPa. The precipitates were then cooled to room temperature and subsequently collected, washed with distilled water and ethanol three times. The precipitates were then dried in a drying oven at 60° C for 24 h.

2.1.2. Microwave-assisted synthesis with methionine

The synthesis is similar to the previous one. The difference is the initial preparation of complexes of Ca^{2+} and Tb^{3+} with methionine as complex agent as described with other ions [28].

2.1.3. Co-precipitation synthesis

We used $CaCl_2$, $Na_2WO_4{\cdot}2H_2O$, $TbCl_3{\cdot}6H_2O$, and s ethylenediaminetetraacetic acid disodium salt (EDTA-Na_2) as the starting materials, and all of them were of analytical grade. Sodium tungstate was dissolved in water and stirred for 30 min at 80 °C. Calcium and terbium chlorides were dissolved in a separate flask in an equal amount of water and also stirred for 30 min at 80 °C. The chloride solution was added dropwise with heating and stirring to the tungstate solution and mixed for 30 min. The substance was washed 3 times with distilled water and ethanol. They were dried for 24 h at 60 °C. Then samples were calcined for 5 h at 400 °C.

2.1.4. Ultrasonic-assisted synthesis

We used $CaCl_2$, $Na_2WO_4{\cdot}2H_2O$, and $TbCl_3{\cdot}6H_2O$ used as the starting materials, and all were of analytical grade. The $CaWO_4$:10 %Tb^{3+} nanocrystals were prepared using the ultrasonic-assisted method described in [23]. In a typical procedure, 0.0167 mol of $CaCl_2$ and $TbCl_3$ were dissolved separately from $Na_2WO_4{\cdot}2H_2O$ in deionized water (DI) by continuously stirring until the transparent solution was prepared. After that, two solutions were added to the chamber of Sonics Vibra-Cell Processor VCX750 and the ultrasonic probe (10 mm diameter; Ti-horn) was immersed with the frequency of pulsed ultrasound waves (conducted in the 2 s mode, and a pause in the 1 s mode) at 50 kHz and 40 W/cm^2. White precipitate particles were washed with distilled water several times and then with absolute ethanol before drying at 60 °C for 24 h.

2.2. Characterization

The X-ray diffraction (XRD) of the synthesized nanoparticles was measured by the D2 PHASER diffractometer (Bruker AXS Inc., USA) using Cu Kα = radiation (λ = 1.5406 Å) at 30 kV and 10 mA. For the measurements, we used a low-background cuvette and the following conditions: 2θ range – 5°–60°, step size – 0.01°.

The elemental composition was analyzed using X-ray microfluorescence spectrometer M4 Tornado 2D (Bruker, USA) with XFlash 430 detector. The analysis was carried out in a multipoint regime for 20 points with measurement time at one point 10 s.

X-ray excited optical luminescence (XEOL) signals were collected using Cary Eclipse fluorimeter (Agelent, USA) and an X-ray tube as a source of ionizing radiation. The fluorimeter emission slit was set to 10 nm and the gate time of 0.1 s per point was utilized. The samples in a powder form were deposited on the plastic holder forming a thin layer with a thickness of 0.4 mm. The X-ray tube was operated at 35 kV and 1.6 mA.

3. Results and discussion

3.1. X-ray diffraction (XRD)

The results of the XRD analysis show that the samples obtained in the reaction with methionine have characteristic diffraction peaks of two phases: scheelite and methionine. Other samples are single-phase, and all phases can be associated with a scheelite-type structure. However, taking into account the different intensity and width of the peaks observed, it is possible to assume the different crystallinity of the samples.Fig. 1

The FW1/5M−FW4/5M method was used to assess the degree of crystallinity of the samples, crystallite sizes, and grain size distribution [29]. This method has several advantages over the conventional Scherrer method [30]. The width of the each peak, in addition to the crystallites size, is also influenced by the instrumental errors of the diffractometer. As a consequence, when only one peaks FWHM is used, these errors affect the result. The FW1/5M -FW4/5M method uses the two widths of each peak and their ratio, so instrumental errors can be concealed [31]. But the only significant factor that depends on the crystallite size is retained, the change in the width of the peak at the base and the apex. Measurement of two widths of the same peak makes it possible to calculate, in addition to the average grain size < R>, also the size variance σ. These parameters are sufficient to draw a grain size distribution (GSD) curve that is much more informative than a single medium < R > parameter. The direct calculation of the average particle size and dispersion is performed using the following formulas described in [29]. The calculated average particle size and size dispersion are presented in Table 1. The particle size distribution is shown in Fig. 2.

As can be seen from the data obtained, the most uniform particle size distribution can be obtained using the ultrasonic-assisted method: the smallest relative distribution width and the particle size are not more than 40 nm. In other cases, despite the possibility of obtaining more nanosized particles of the order of 5–20 nm in the bulk, the distribution shows the presence of larger particles of the order of 60–100 nm (Fig. 2).

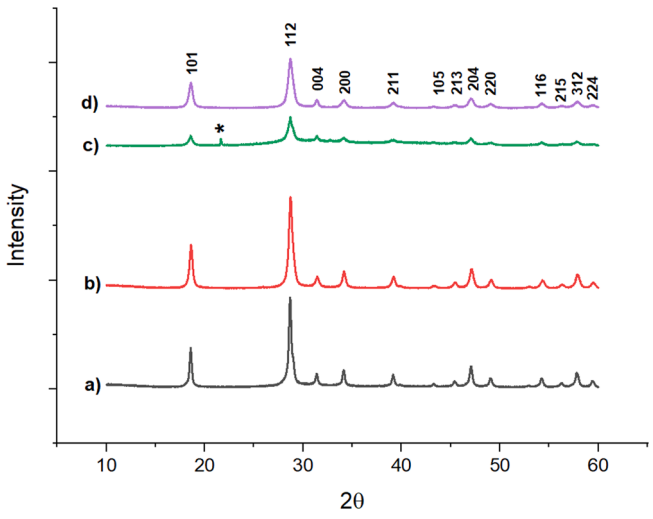

Fig. 1. X-ray diffraction pattern of $CaWO_4$:x%Tb^{3+} synthesized by: a) co-precipitation method; b) microwave-assisted method; c) microwave-assisted with methionine (methionine peak is marked by a star; d) ultrasonic-assisted method.

Table 1
The results of processing diffraction patterns by the FW1/5M−FW4/5M method for samples with different synthesis conditions.

Method of synthesis	Size average, <R> [nm]	Size dispersion, σ [nm]	Relative width, σ / <R>
Co-precipitation	28.4	21.1	0.74
Microwave-assisted	24.5	9.1	0.37
Ultrasonic-assisted	19.0	6.3	0.33
Microwave-assisted with methionine	20.0	11.5	0.58

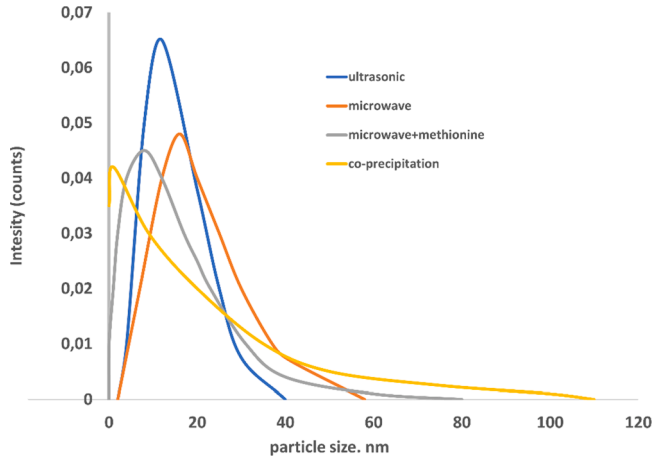

Fig. 2. Grain size distribution for samples of $CaWO_4$:x%Tb^{3+} obtained by different methods.

Therefore, to obtain a product with a more uniform microstructure, the ultrasonic method of synthesis is preferable.

3.2. X-ray fluorescence (XRF)

The elemental composition of the synthesized materials determined by X-ray fluorescence (XRF) analysis is presented in Table 2. As can be seen, in three synthesis methods, it is possible to achieve the substitution of calcium for terbium by 10 mol%, with a slight calcium deficiency in the structure. Along with the absence of any side products traces observed from XRD and single-phase character of the materials, XRF data confirms that terbium is embedded in the scheelite structure. The only synthesis method where complete substitution has not been achieved is microwave synthesis using amino acids as a complexing agent to prevent rapid precipitation. In this case, it was possible to achieve the substitution of only 3 mol% calcium. Perhaps this is due to the formation of strong complexes of terbium and amino acids in solution. Thus, the molar ratio of the elements in the formula is 0.75: 0.1: 1 in the first three cases and 0.77: 0.03: 1 in the case of methionine.

Table 2
Elemental composition of the samples with formula $CaWO_4$:Tb^{3+} measured by XRF.

Methods of synthesis	Elemental composition, at.% by XRF		
	Ca	Tb	W
Co-precipitation	40.56	5.16	54.28
Microwave-assisted	41.11	5.06	54.91
Ultrasonic-assisted	38.80	6.37	54.83
Microwave-assisted with methionine	43.73	1.66	56.61

3.3. X-ray emission optical luminescence (XEOL)

XEOL spectra are shown in Fig. 3. We will start the discussion from the signal observed for the MW-synthesized sample. The XEOL spectrum characterized by the four bands typical for Tb^{3+} ion, which are observed due to $4f^8$-$4f^8$ transitions: $^5D_4 \rightarrow {}^7F_6$ (λ = 490 nm), $^5D_4 \rightarrow {}^7F_5$ (λ = 545 nm), $^5D_4 \rightarrow {}^7F_4$ (λ = 585 nm), and $^5D_3 \rightarrow {}^7F_6$ (λ = 621 nm). While the broad maximum observed in the blue range of the spectra is associated with the 5*d*-2*p* emission of the WO_4^{2-} group [32]. As it has been recently demonstrated by Guo et al. [32], due to the intrinsic electronic transition of heavy W (np_6-nd), the WO_4^{2-} groups being coupled with RE elements can serve as efficient X-ray scintillator. However, in our case the decrease in the WO_4^{2-} broad peak intensity observed for MW-methionine and ultrasonic synthesis is accompanied by the decrease in green Tb^{3+} luminescence, thus it cannot be associated with more efficient tungstate host – Tb^{3+} energy transfer. Therefore we suggest that the observed loss of intensity is associated with particle size and morphology obtained in different syntheses. Moreover, in the case of the MW-methionine sample the lower Tb^{3+} luminescence is expected due to a substantially lower amount of Tb in the structure as obtained from XRF analysis (See Table 2). While almost zero intensity in the WO_4^{2-} luminescence range is rather surprising and might be related to very small particle sizes.

Intensive WO_4^{2-} luminescence has been also observed for the sample obtained by co-precipitation. Interestingly that compare with MW synthesis, this sample demonstrates the substantially higher intensity of the main Tb^{3+} lines (green luminescence). Moreover, for this sample blue emission of Tb^{3+} has been also observed, which appears as a sequence of well-defined peaks overlapped with broad WO_4^{2-} feature. These peaks might be associated with the transition from $^5D_3$ to ^7F_J levels [33-35]. As recently reported by Linganna and co-workers [35] the observed emission from the $^5D_3$ level might be related to slow non-radiative relaxation from $^5D_3$ to $^5D_4$ accompanied by the cross-relaxation of Tb^{3+}. The higher intensity of the typical green Tb^{3+} luminescence and the appearance of blue Tb^{3+} emission components assume the higher crystallinity of the particles obtained by the co-precipitation method and likely higher symmetry of the luminescence Tb sites.

To sum up, the effect of different synthesis methods, we can declare that those methods which yield a large variance in the particle sizes exhibit a higher intensity of the XEOL signal. Hence within the methods considered in this work microwave and coprecipitation methods are preferred due to higher scintillating efficiency.

As can be seen from the graph, the samples obtained by the coprecipitation method have the highest intensity, and those obtained by synthesis with methionine have the least intensity. However, the last

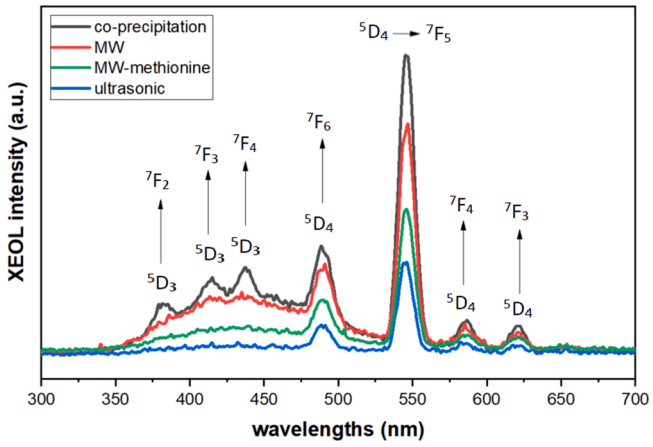

Fig. 3. XEOL spectra collected for samples obtained by different synthesis routes. The peaks which correspond to Tb^{3+} luminescence are marked on the plot, while the broad maximum in the range 350–500 nm is associated with WO_4^{2-} luminescence.

sample should be excluded from the general comparison because it is multiphase and differs in the content of Tb^{3+}. Its low intensity is apparently related to the low content of Tb^{3+} in the composition.

The remaining three samples can be compared in terms of the effect of different synthesis routes using the average calculated particle size from the Table 1 as a parameter. In this case, a fairly simple correlation is obtained: The larger the average particle size, the higher the intensity of the XEOL spectra. On the other hand, as can be seen from Fig. 2, the particle size distribution is not exactly the same for different syntheses, and we consider it important to discuss it. In the case of synthesis by coprecipitation, we have the largest dispersion in size from 3 to 100 nm, and both smaller and larger particles can enhance the radiation and possibly have a joint effect. On the other hand, the sample with the lowest intensity has the lowest particle size dispersion from 3 to 37 nm. That is, particles with very similar sizes contribute to the observed averaged signal. In the case then intensity of XEOL spectrum is intermediate i.e. microwave synthesis, the particle size distribution is also intermediate. Since the average particle size is a somewhat arbitrary value, it seems to us that more universal parameters can be used to assess the effect of particles dimension on spectra - the size range and its dispersion. The exact dependence of the effect of sizes less than 10 nm and more than 100 nm can be obtained in further experiments on XEOL measurements of particles separated with narrow size distribution peaking at different values and obtained by the same synthesis method.

If we summarize the data on the effect of the synthesis method, then we can say that methods that give a large grain size give a high intensity in the spectra. Hence microwave and coprecipitation are preferred.

4. Conclusion

This paper has shown that the size of the crystallites and the GSD for CaWO4:10 %Tb3 + influence the intensity of the XEOL spectra. These data can be used for a more precise search for materials for X-PDT. The main advantage of lanthanide-substituted calcium tungstate is the combination of luminescence not only from terbium cations. This combination allows one to increase choice of the photosensitizer. The results of this study also underline what methods of synthesis allow us to obtain particles with different size distributions. Ultrasonic-assisted methods are preferable to synthesize nearly monodispersed particles.

Funding

Research was financially supported by the Ministry of Science and Higher Education of the Russian Federation (State assignment in the field of scientific activity, № 0852-2020-0019).

CRediT authorship contribution statement

E.A Mukhanova: Conceptualization, Writing – original draft, Writing – review & editing. **I.A. Pankin:** Data curation, Visualization, Writing – original draft. **O.E. Polozhentsev:** Data curation, Writing – review & editing. **P.D. Kuznetsova:** Data curation, Validation. **V.A. Polyakov:** Data curation, Validation. **A.V. Soldatov:** Conceptualization, Project administration.

Declaration of Competing Interest

The authors declare that they have no known competing financial interests or personal relationships that could have appeared to influence the work reported in this paper.

Acknowledgement

This research was financially supported by the Ministry of Science and Higher Education of the Russian Federation (State assignment in the field of scientific activity, No 0852-2020-0019).

References

[1] P. Agostinis, K. Berg, K.A. Cengel, T.H. Foster, A.W. Girotti, S.O. Gollnick, S. M. Hahn, M.R. Hamblin, A. Juzeniene, D. Kessel, M. Korbelik, J. Moan, P. Mroz, D. Nowis, J. Piette, B.C. Wilson, J. Golab, Photodynamic therapy of cancer: An update, CA, Cancer J. Clin. 61 (4) (2011) 250–281, https://doi.org/10.3322/caac.20114.

[2] M.A. Calin, S.V. Parasca, Photodynamic therapy in oncology, J. Optoelectron. Adv. Mater. 8 (2006) 1173–1179, https://doi.org/10.1634/theoncologist.11-9-1034.

[3] A.F. Dos Santos, D.R.Q. De Almeida, L.F. Terra, M.S. Baptista, L. Labriola, Photodynamic therapy in cancer treatment - an update review, J. Cancer Metastasis Treat. 2019 (2019), https://doi.org/10.20517/2394-4722.2018.83.

[4] S. Kwiatkowski, B. Knap, D. Przystupski, J. Saczko, E. Kędzierska, K. Knap-Czop, J. Kotlińska, O. Michel, K. Kotowski, J. Kulbacka, Photodynamic therapy – mechanisms, photosensitizers and combinations, Biomed. Pharmacother. 106 (2018) 1098–1107, https://doi.org/10.1016/j.biopha.2018.07.049.

[5] J. Chen, T. Fan, Z. Xie, Q. Zeng, P. Xue, T. Zheng, Y. Chen, X. Luo, H. Zhang, Advances in nanomaterials for photodynamic therapy applications: Status and challenges, Biomaterials 237 (2020) 119827, https://doi.org/10.1016/j.biomaterials.2020.119827.

[6] M. Lan, S. Zhao, W. Liu, C.-S. Lee, W. Zhang, P. Wang, Photosensitizers for Photodynamic Therapy, Adv. Healthc. Mater. 8 (13) (2019) 1900132, https://doi.org/10.1002/adhm.201900132.

[7] J. Xie, Y. Wang, W. Choi, P. Jangili, Y. Ge, Y. Xu, J. Kang, L. Liu, B. Zhang, Z. Xie, J. He, N.i. Xie, G. Nie, H. Zhang, J.S. Kim, Overcoming barriers in photodynamic therapy harnessing nano-formulation strategies, Chem. Soc. Rev. 50 (16) (2021) 9152–9201, https://doi.org/10.1039/D0CS01370F.

[8] S. Shrestha, J. Wu, B. Sah, A. Vanasse, L.N. Cooper, L. Ma, G. Li, H. Zheng, W. Chen, M.P. Antosh, X-ray induced photodynamic therapy with copper-cysteamine nanoparticles in mice tumors, Proc. Natl. Acad. Sci. 116 (34) (2019) 16823–16828, https://doi.org/10.1073/pnas.1900502116.

[9] W. Sun, Z. Zhou, G. Pratx, X. Chen, H. Chen, Nanoscintillator-mediated X-ray induced photodynamic therapy for deep-seated tumors: from concept to biomedical applications, Theranostics 10 (3) (2020) 1296–1318, https://doi.org/10.7150/thno.41578.

[10] S. Ling, J. Gao, G. Chu, J. Huang, R. Xiao, C. Ouyang, H. Li, L. Chen, Application of high-throughput calculations for screening lithium battery materials, Mater. China. 34 (2015) 272–281, https://doi.org/10.7502/j.issn.1674-3962.2015.04.03.

[11] L. Ma, X. Zou, W. Chen, A new X-ray activated nanoparticle photosensitizer for cancer treatment, J. Biomed. Nanotechnol. 10 (8) (2014) 1501–1508, https://doi.org/10.1166/jbn.2014.1954.

[12] S. Yekta, M. Sadeghi, E. Babanezhad, Synthesis of $CaWO_4$ nanoparticles and its application for the adsorption-degradation of organophosphorus cyanophos, J. Water Process Eng. 14 (2016) 19–27, https://doi.org/10.1016/j.jwpe.2016.10.004.

[13] J. Lee, N.J. Rancilio, J.M. Poulson, Y.-Y. Won, Block copolymer-encapsulated $CaWO_4$ nanoparticles: synthesis, formulation, and characterization, ACS Appl. Mater. Interfaces. 8 (13) (2016) 8608–8619, https://doi.org/10.1021/acsami.6b0072710.1021/acsami.6b00727.s001.

[14] J.Y.P. Ko, Y. Hu, L. Armelao, T.-K. Sham, XANES and XEOL studies of Eu-doped calcium tungstate in silica synthesized by sol-gel method, J. Phys. Conf. Ser. 190 (2009) 012078, https://doi.org/10.1088/1742-6596/190/1/012078.

[15] J. Lee, N.J. Rancilio, J.M. Poulson, Y.-Y. Won, Block copolymer-encapsulated $CaWO_4$ nanoparticles: synthesis, formulation, and characterization, ACS Appl. Mater. Interfaces. 8 (13) (2016) 8608–8619, https://doi.org/10.1021/acsami.6b0072710.1021/acsami.6b00727.s001.

[16] B. Grobelna, B. Lipowska, A.M. Kłonkowski, Energy transfer in calcium tungstate doped with Eu(III) or Tb(III) ions incorporated into silica xerogel, J. Alloys Compd. 419 (1-2) (2006) 191–196, https://doi.org/10.1016/j.jallcom.2005.07.078.

[17] F.S.M. Canisares, A.M.G. Mutti, D.G.S.M. Cavalcante, A.E. Job, A.M. Pires, S.A. M. Lima, Luminescence and cytotoxic study of red emissive europium(III) complex as a cell dye, J. Photochem. Photobiol. A Chem. 422 (2022) 113552, https://doi.org/10.1016/j.jphotochem.2021.113552.

[18] A. Shahedi, M.A. Bolorizadeh, H. Karimi-Maleh, A europium (III) complex tested for deoxyribonucleic acid-binding, bovine serum albumin binding, and antibacterial activity, J. Mol. Liq. 335 (2021) 116323, https://doi.org/10.1016/j.molliq.2021.116323.

[19] J. Jessat, S. Sachs, H. Moll, W. John, R. Steudtner, R. Hübner, F. Bok, T. Stumpf, Bioassociation of U(VI) and Eu(III) by Plant (Brassica napus) Suspension Cell Cultures—A Spectroscopic Investigation, Environ. Sci. Technol. 55 (10) (2021) 6718–6728, https://doi.org/10.1021/acs.est.0c05881.

[20] H. Moll, S. Sachs, G. Geipel, Plant cell (Brassica napus) response to europium(III) and uranium(VI) exposure, Environ. Sci. Pollut. Res. 27 (25) (2020) 32048–32061, https://doi.org/10.1007/s11356-020-09525-2.

[21] S.K. Nethi, A.K. Barui, P. Jhelum, P. Basuthakur, V.S. Bollu, B.R. Reddy, S. Chakravarty, C.R. Patra, Europium Hydroxide Nanorods Mitigate Hind Limb Ischemia in Wistar Rats, Adv. Ther. 4 (6) (2021) 2100016, https://doi.org/10.1002/adtp.202100016.

[22] R.E. Izzaty, B. Astuti, N. Cholimah, Circularly Polarized Luminescence from Terbium(II1) as a Probe of Metal Ion Binding in Calcium-Binding Proteins, Angew. Chemie Int. Ed. 6(11), 951–952. (1967) 5–24.

[23] J. Janbua, J. Mayamae, S. Wirunchit, R. Baitahe, N. Vittayakorn, Directed synthesis, growth process and optical properties of monodispersed CaWO 4 microspheres via a sonochemical route, RSC Adv. 5 (26) (2015) 19893–19899, https://doi.org/10.1039/C4RA15064C.

[24] M.E.M. Li, T. Jüstel, M. Neukirch, H. Bettentrup, J. Plewa, D. Uhlich, T. Jüstel, M. Neukirch, H. Meyer, S. Germany, Effect of Alkaline Cation Type and Preparation Method on the Formation of Effect of Alkaline Cation Type and Preparation Method on the Formation of $MLaW_2O_8$: Eu (M = Li , Na , K , Rb, Cs), (2007).
[25] S.K. Gupta, Y. Mao, Recent advances, challenges, and opportunities of inorganic nanoscintillators, Front. Optoelectron. 13 (2) (2020) 156–187, https://doi.org/10.1007/s12200-020-1003-5.
[26] P.K. Sharma, R.K. Dutta, A.C. Pandey, Size-dependent emission efficiency and luminescence characteristics of YBO_3: Tb^{3+} nanocrystals under vacuum ultraviolet excitations, J. Appl. Phys. 112 (2012) 2–6, https://doi.org/10.1063/1.4751335.
[27] Y.-C. Chang, C.-Y. Lee, H.-T. Chiu, Porous inorganic materials from living porogens: channel-like TiO_2 from yeast-assisted sol-gel process, ACS Appl. Mater. Interfaces. 6 (1) (2014) 31–35, https://doi.org/10.1021/am405149a.
[28] F. Zereini, C.L.S. Wiseman, M. Vang, P. Albers, W. Schneider, R. Schindl, K. Leopold, Geochemical behaviour of palladium in soils and Pd/PdO model substances in the presence of the organic complexing agents <scp>l</scp> -methionine and citric acid, Environ. Sci. Process. Impacts. 18 (2016) 22–31, https://doi.org/10.1039/C5EM00521C.
[29] R. Pielaszek, FW/M method for determination of the grain size distribution from powder diffraction line profile, J. Alloys Compd. 382 (1-2) (2004) 128–132, https://doi.org/10.1016/j.jallcom.2004.05.040.
[30] A.L. Patterson, The Scherrer Formula for X-Ray Particle Size Determination, Phys. Rev. 56 (10) (1939) 978–982, https://doi.org/10.1103/PhysRev.56.978.
[31] J. Wojnarowicz, R. Mukhovskyi, E. Pietrzykowska, Microwave solvothermal synthesis and characterization of manganese-doped ZnO nanoparticles, (2016). https://doi.org/10.3762/bjnano.7.64.
[32] T. Guo, Y. Lin, W.-J. Zhang, J.-S. Hong, R.-H. Lin, X.-P. Wu, J. Li, C.-H. Lu, H.-H. Yang, High-efficiency X-ray luminescence in Eu 3+ -activated tungstate nanoprobes for optical imaging through energy transfer sensitization, Nanoscale 10 (4) (2018) 1607–1612, https://doi.org/10.1039/C7NR06405E.
[33] J. Juárez-Batalla, A.N. Meza-Rocha, G.H. Muñoz, I. Camarillo, U. Caldiño, Luminescence properties of Tb^{3+}-doped zinc phosphate glasses for green laser application, Opt. Mater. (Amst). 58 (2016) 406–411, https://doi.org/10.1016/j.optmat.2016.06.022.
[34] N. Wada, K. Kojima, Decay behavior of Tb3+ green fluorescence in borate glasses, Opt. Mater. (Amst) 35 (11) (2013) 1908–1913, https://doi.org/10.1016/j.optmat.2013.01.008.
[35] K. Linganna, S. Ju, C.h. Basavapoornima, V. Venkatramu, C.K. Jayasankar, Luminescence and decay characteristics of Tb^{3+} -doped fluorophosphate glasses, J. Asian Ceram. Soc. 6 (1) (2018) 82–87, https://doi.org/10.1080/21870764.2018.1442674.